

Observation of Extreme Phase Transition Temperatures of Water Confined Inside Isolated Carbon Nanotubes

Kumar Varoon Agrawal[†], Steven Shimizu[†], Lee W. Drahushuk, Daniel Kilcoyne and
Michael S. Strano

Department of Chemical Engineering, Massachusetts Institute of Technology, Cambridge, Massachusetts

NATURE NANOTECHNOLOGY DOI: 10.1038/NNANO.2016.254

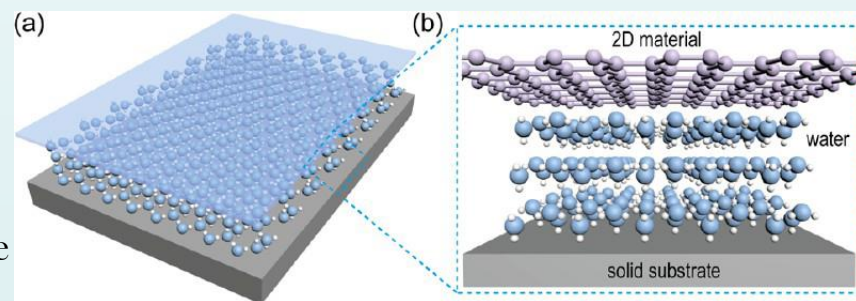
by,

S.Vidhya

07.01.2017

Introduction

- Water can be found in the bulk form but is also present within confined environments.
- Confined water at the nanoscale has different dynamics and structures from that of the bulk water
- The physical properties and the state of the confined water have been proven to be widely varied depending on the cavity surface and the confinement dimensions, as well as temperature and pressure.
- The interface between water and other materials under ambient conditions is of fundamental importance due to its relevance in daily life and a broad range of scientific research.
- The behavior of confined water at the nanoscale under ambient conditions is still not fully understood.
- The reasons are twofold: first, most knowledge of water structures at interfaces has been gained at cryogenic temperatures and under ultrahigh-vacuum conditions, which might not be transferable to ambient conditions
- Second, direct microscopic imaging of wetting dynamics of water confined in nanoscale geometries remains challenging.



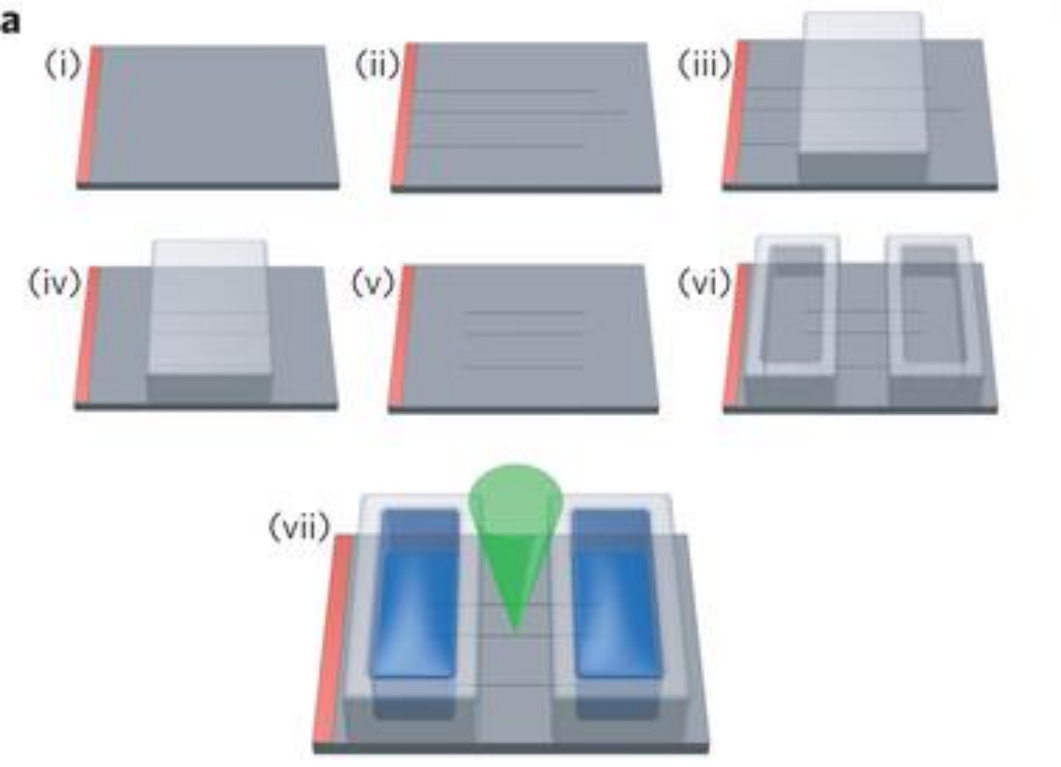
Introduction

- ❖ Water confined to nanometre-sized pores, such as the interior of a carbon nanotube (CNT) exhibits unusual phase behaviour due to confinement effects.
- ❖ When confined inside sub-1.5 nm diameter CNTs, water can freeze to form ice NTs.
- ❖ Such tubes are of fundamental scientific interest, and attractive as potential nanoscale ferroelectric devices, gas nanovalves, nanoscale flow sensors and high-flux membranes.
- ❖ Molecular simulations predict that confined water in CNT can freeze above 0 °C, approaching room temperature, making hydrated CNTs a possible candidate for a latent heat thermal storage system.
- ❖ Generally, the understanding of fluid phase transitions inside CNTs has been limited to reports based on molecular dynamics (MD) simulations and experiments on polydisperse powders and suspensions of CNTs. Typically, MD simulations are subjected to the limitations of force field accuracy. On the other hand, experiments on polydisperse CNTs greatly reduce the resolution of the diameter dependent behaviour of confined water.
- ❖ Water in 0.8-1.0 nm CNT pores has been shown to exist in a vapour-like, entropically stabilized state.
- ❖ Simulations predict that between 1.1 and 1.2 nm, stabilization becomes enthalpic with an ice-like phase, followed by a bulk-like liquid phase stabilization for tubes larger than 1.4 nm in diameter.

Introduction

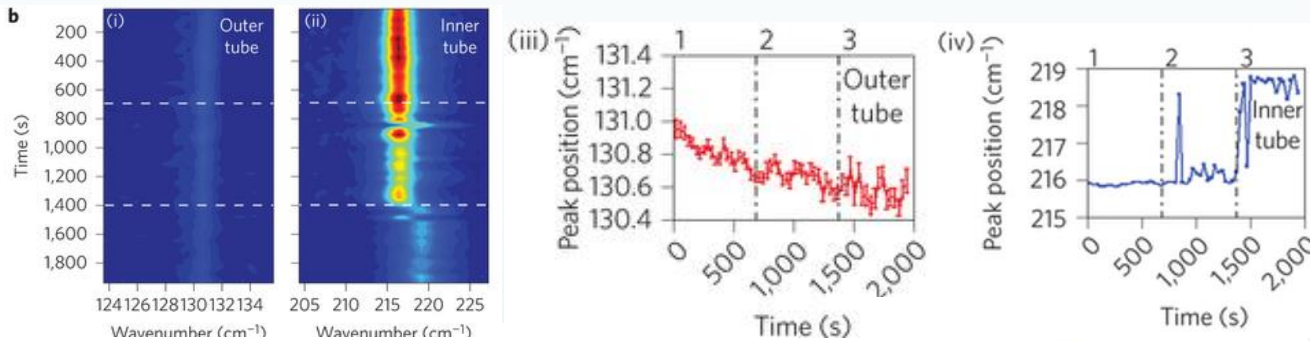
- In this paper, two different techniques have been used to explore the diameter-dependent phase boundaries of ice NTs formed within isolated CNTs over a range of diameters from 1.05 to 1.52 nm.
- It is shown that the phase behaviour of water inside the single-walled and double-walled nanotubes can be monitored using the dynamic shift in the frequency of the Raman radial breathing mode (RBM).
- This feature is used to study fluid phase filling and reversible freezing transitions at temperatures higher than 100 °C.
- This study demonstrates that the phase transitions of confined water in CNTs are extremely diameter-dependent, and freezing transitions as high as 138 °C for 1.05 nm metallic SWNTs were observed, close to the range of enthalpy stabilized, ice-like water.
- A laser-heating model has been then utilized to show that aqueous filling of the CNT substantially reduces the axial thermal conductivity (k_a), providing a means of reversibly switching the heat flux in the conduit.

Experimental

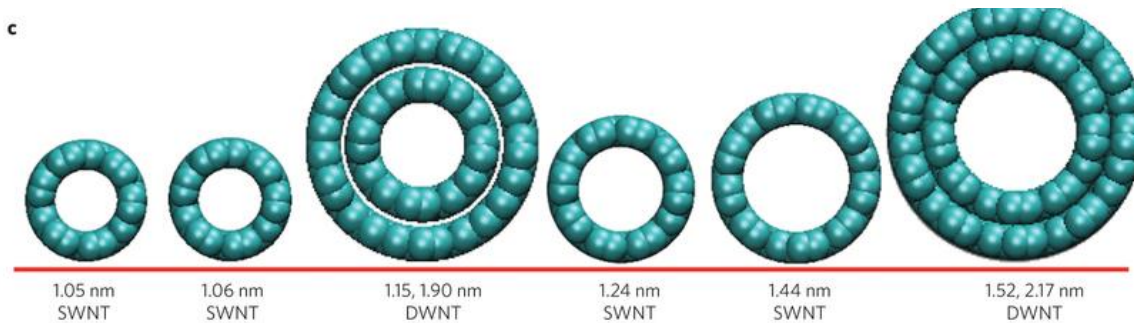


a, Fabrication of the platform, which comprises isolated CNTs connected to two reservoirs. (i) A catalyst solution consisting of iron nanoparticles (red) is deposited along an edge of the Si substrate. (ii) Centimere-long, horizontally aligned CNTs are grown using CVD with methane. (iii) A PDMS protective mask is placed on the middle section of the CNTs. (iv) Air plasma removes the uncovered parts of the CNTs, opening up the ends. (v) The PDMS mask is removed. (vi) Two PDMS reservoirs are adhered to the surface. (vii) The reservoirs are filled with water and microRaman spectroscopy is performed on the CNT.

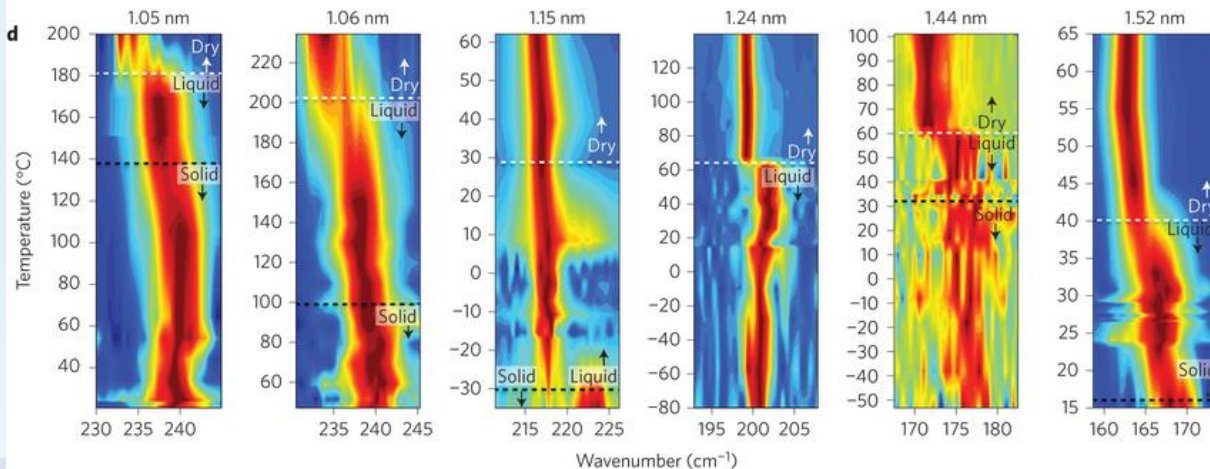
Evidence of filling and phase transition of water inside CNTs



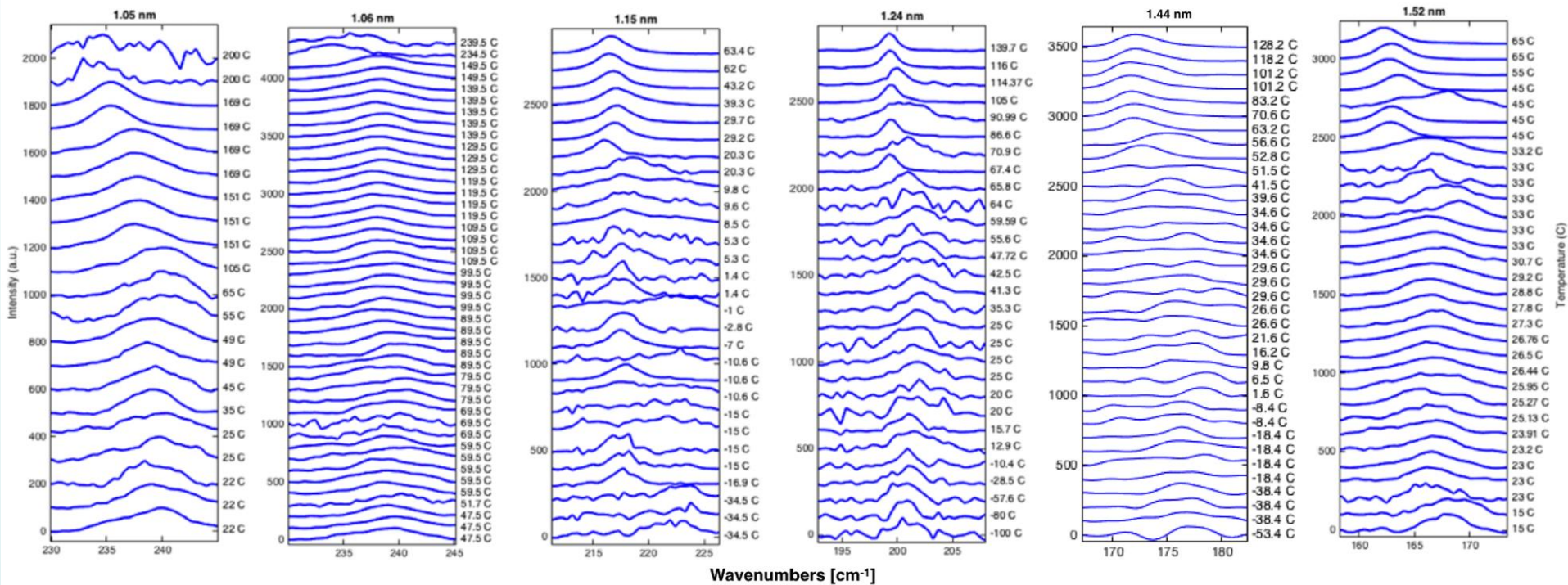
b, Temporal study of the RBM frequency. (i,ii) A time-map showing the evolution of RBM frequency and intensities for the 1.15 nm DWNT. Dotted lines indicate the time points at which water is added to the reservoirs. (iii,iv) Fitted peak positions for the outer and inner RBMs, respectively. 1, reservoirs empty; 2, water added to right reservoir; 3, water added to left reservoir.



c, A visual MD model of the CNTs studied here. The 1.06 nm SWNT was bundled with a 1.55 nm SWNT. d, A contour plot of the representative RBM frequency (based on the signal-to-noise ratio) versus temperature for the six tubes studied here. The white line represents the transition from the dry to the water-filled state, whereas the black line signifies the freezing transition of the confined water.

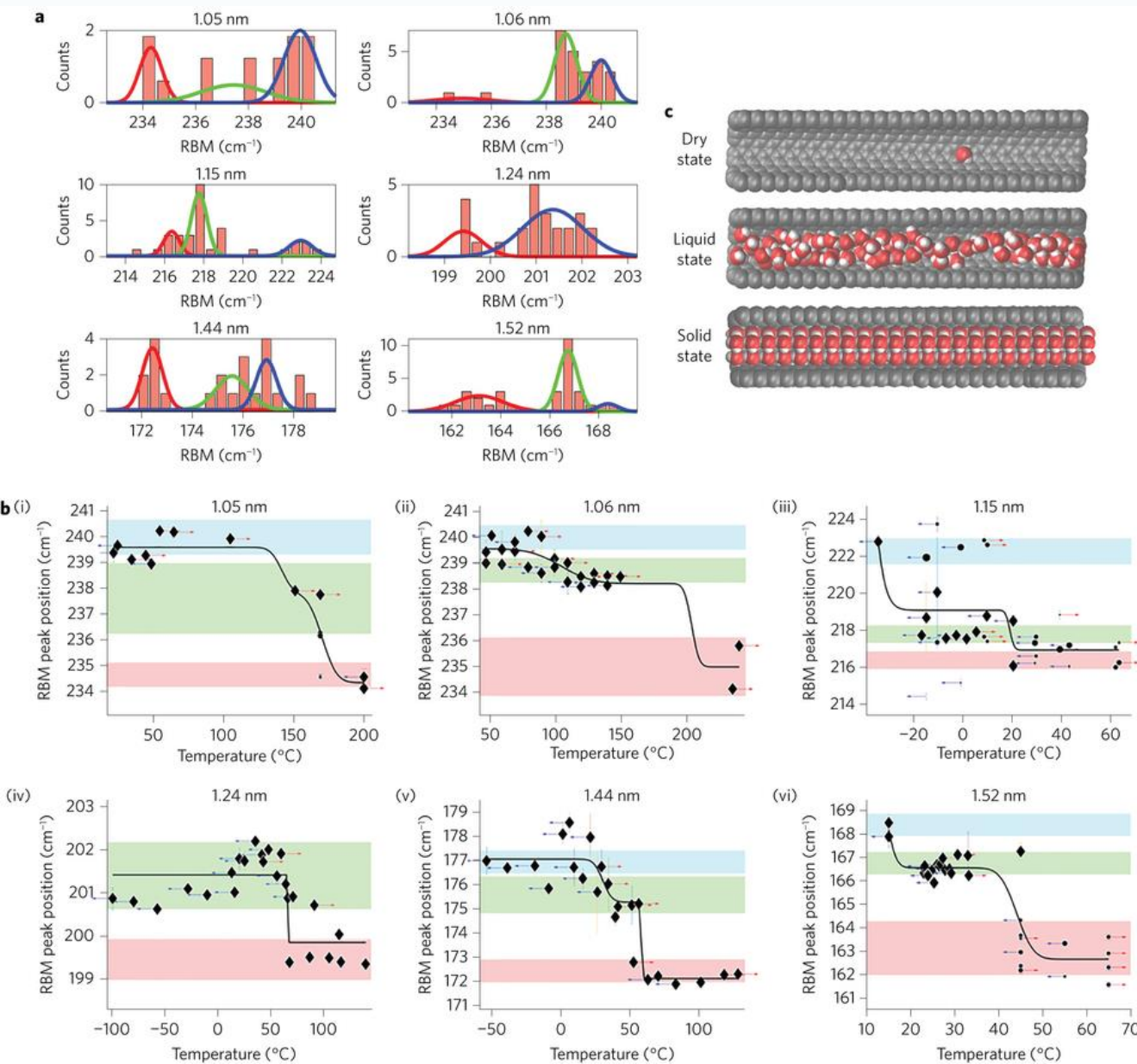


Water velocity based on temporal shift of RBM frequency - $18 \mu\text{s}^{-1}$
 Calculated flow - $13 \mu\text{s}^{-1}$



The complete micro-Raman spectroscopic dataset (RBM frequency vs. intensity) used for the analysis of the phase transition temperature for the 6 CNTs (Finite-width Heaviside function in Fig. 2b). RBM peak intensities have been normalized for the comparison. Note that the analysis of the phase transition temperature in the main text (Fig. 2a and b) is carried out based on this entire dataset. The spectra for contour plot in Fig. 1d are picked from this dataset based on the signal/noise ratio to provide visual cues for the phase transitions.

Diameter-dependent vapour-liquid and liquid-solid phase transitions of confined water inside CNTs

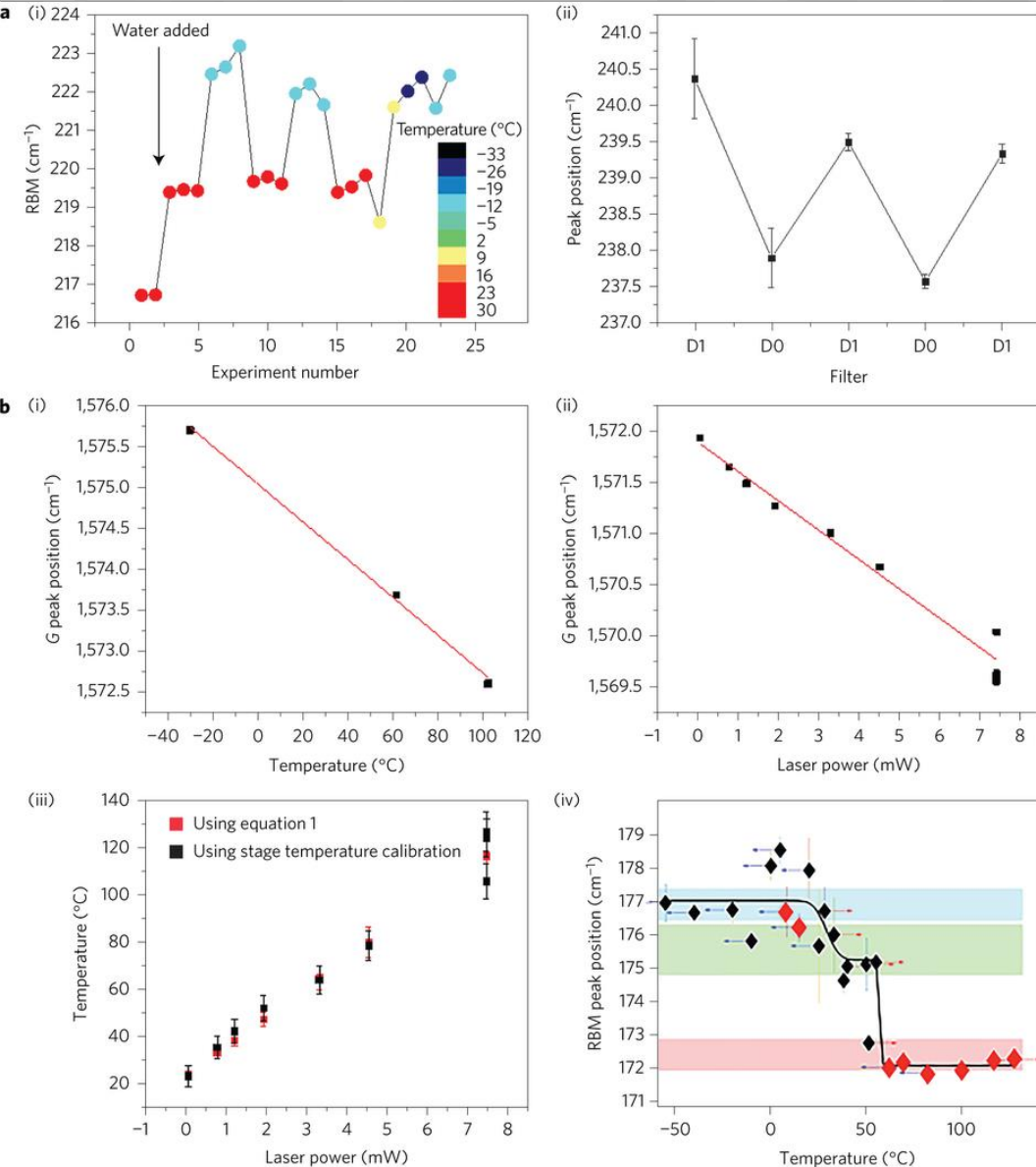


a, Histograms of the RBM peak positions for the six CNTs. Gaussian peaks are fitted to the histogram data, showing up to three peaks that correspond to the distinct states of the CNTs.

b, RBM peak position as a function of tube temperature. A combination of method 1 and method 2 was used to achieve the temperature. Blue left-pointing arrows indicate cooling cycles; red right-pointing arrows indicate heating cycles; the lack of arrows indicates a neutral, starting state. In the case of an RBM peak with a shoulder, we deconvoluted the peaks and the resulting data points are plotted using circular markers with a size that is proportional to the peak area. Single-peak RBMs are represented by the diamond markers. The fitting for deconvoluted data points included weights proportional to the peak area. The shaded brackets correspond to the three states of the CNTs (cyan, solid water; green, liquid water and pink, dry CNTs). The width of each bracket is the FWHM of the peaks fitted to the RBM histogram in a. The black curves are finite-width Heaviside fits. The RBM error bars originate from the error in fitting the RBM peak with a Lorentzian curve.

c, Illustration of the three CNT states.

Reversibility of the water phases inside the CNT on heating and cooling, and agreement in the phase transition data obtained by the two heating methods



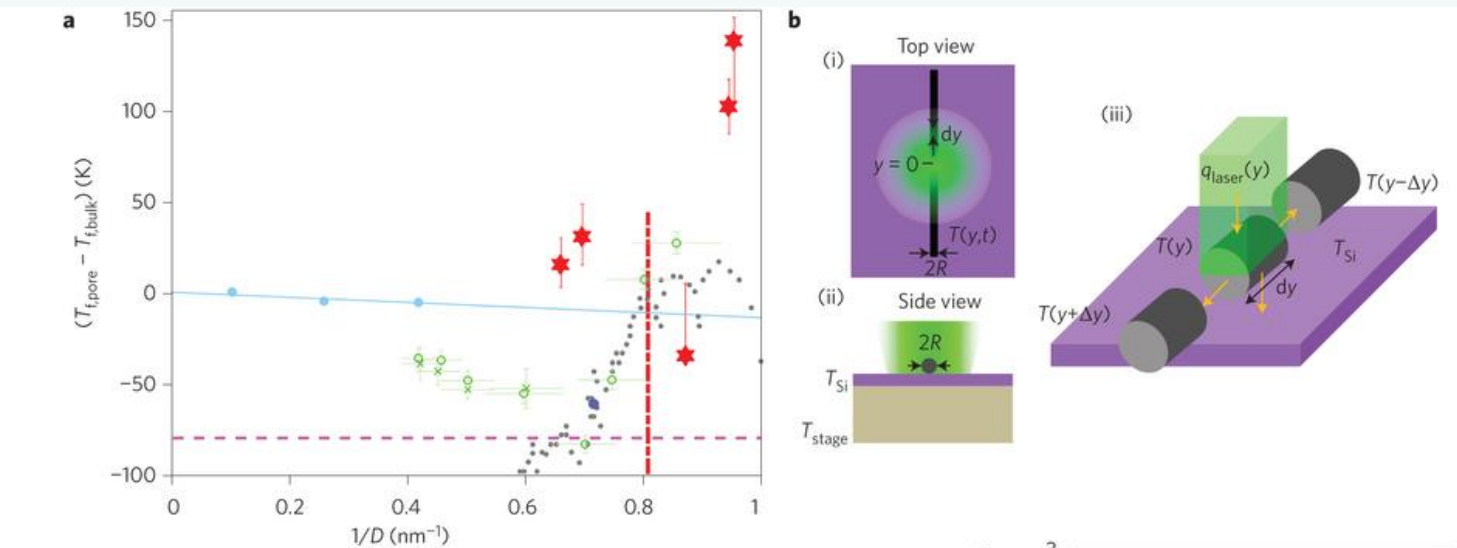
a, RBM frequency of the CNTs as a function of heating and cooling oscillations. (i) The temperature of the 1.15 nm CNT was varied by method 1, changing the stage temperature. (ii) The temperature of the 1.06 nm CNT was varied by method 2, changing laser intensity between the low power 0.8 mW (D1) and the high power 8 mW (D0) modes. The error bars for the peak positions are the errors in fitting them with a Lorentzian curve.

b, (i) Calibration of the G peak position with the stage temperature. (ii) Change in the G peak position as a function of the laser power. (iii) Agreement between temperature calculated by equation (1) and that calculated using the G peak position calibration. The error bars in temperature are errors propagated from errors in χ and β . (iv) A good agreement is found within the phase transition data generated by the two distinct heating methods for a 1.44 nm CNT. Here data highlighted by the black markers refer to method 1 (stage heating) and the red markers refer to method 2 (laser heating). The error bars originate from the errors in fitting the RBM peak positions.

Comparison of the diameter-dependent phase transition temperatures and reduction in the axial conductivity of the CNTs on water filling

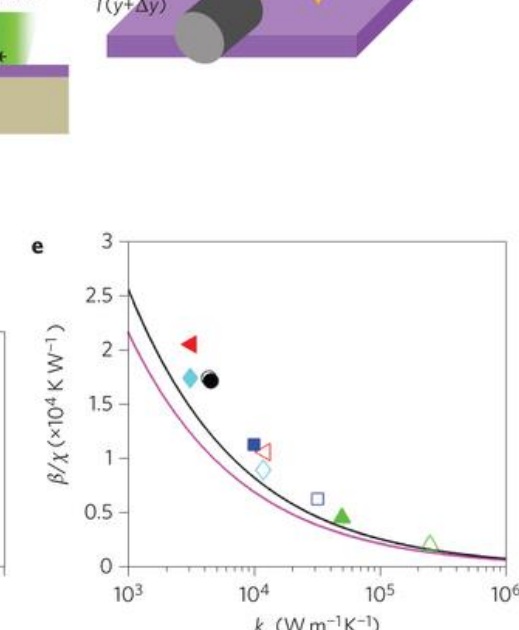
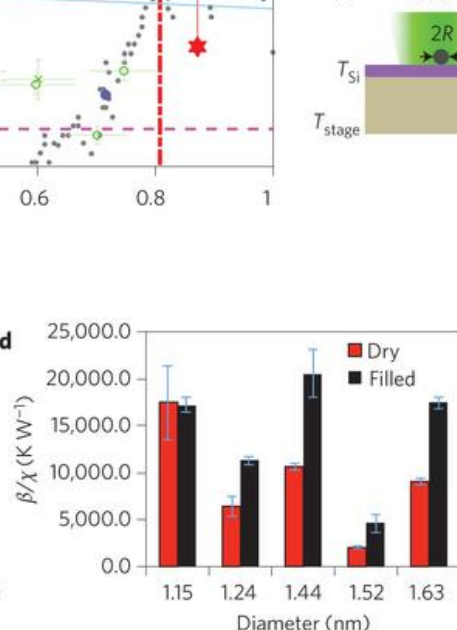
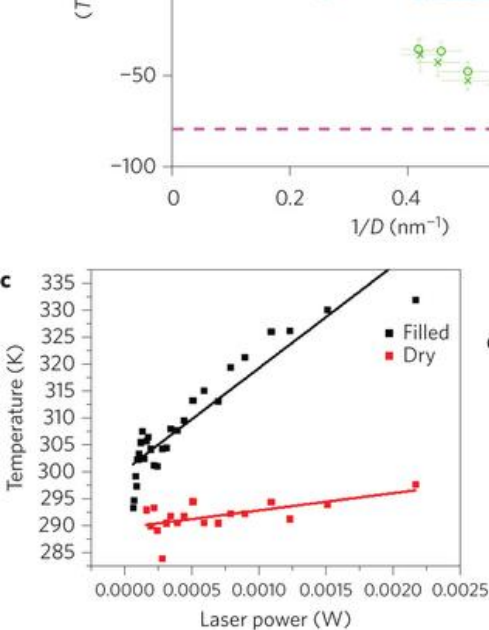
a, A global plot for the freezing point depressions of water confined in CNTs. Red markers indicate experimental data from this work. The error bars in these data originate from the uncertainty in Heaviside fittings in Fig. 2b. The dashed red vertical line represents the 1.24 nm SWNT for which no freezing transition was observed. The dashed magenta horizontal line is the lower temperature bound for the experiment ($-80\text{ }^{\circ}\text{C}$). Cyan markers indicate experimental freezing point depressions for water inside larger MWNTs. The fitted cyan line is the expected trend for freezing point depression as per the Gibbs–Thomson effect. Grey markers indicate the results from the MD simulations on freezing transition of water inside SWNT. The green and blue markers are experimental (XRD and NMR) measurements on polydisperse SWNT powders and suspensions.

b, A schematic for laser heating CNTs on a silicon substrate. (i) A laser is focused on a spot along the length of the tube. This position is defined to be $y = 0$ in the model. (ii) The Si substrate in the experiment is placed on top of a silver heating block. The temperature of the Si substrate, T_{Si} , is assumed to be the same as that of the stage, T_{stage} .



(iii) The energy balance for a differential element of the CNT. Heat from the laser beam, q_{laser} , is dissipated to the colder regions of the CNT, and to the underlying silicon substrate.

c, Local temperature of the 1.24 nm CNT versus the laser power in the filled and dry states.



d, Comparison of β/χ for CNTs in the filled versus dry states.

e, A plot of β/χ versus k_a showing that on filling, CNTs undergo decrease in k_a . The black and the pink curves are obtained from the laser heating model for tubes of 1.15 and 1.63 nm in diameter, respectively. The black, blue, red, green and cyan symbols represent 1.15, 1.24, 1.44, 1.52 and 1.63 nm diameter tubes, respectively. Open symbols represent tubes in the dry state, whereas solid symbols represent tubes in the filled state.

Conclusions

- The phase boundaries of confined water in isolated CNTs of various diameters has been measured, demonstrating a unique and extreme sensitivity to this parameter.
- The results enable the study and application of ice NTs at room temperature and above.
- Diameters that display melting transitions at room temperature, enabling new phase-change materials have been reported.
- The modulation of thermal conductivity with phase change in the interior of the CNTs enables the digital control of heat flux through these nanoconduits.
- Overall, these results underscore new opportunities for phase transitions of confined fluids inside CNTs.

Take Away

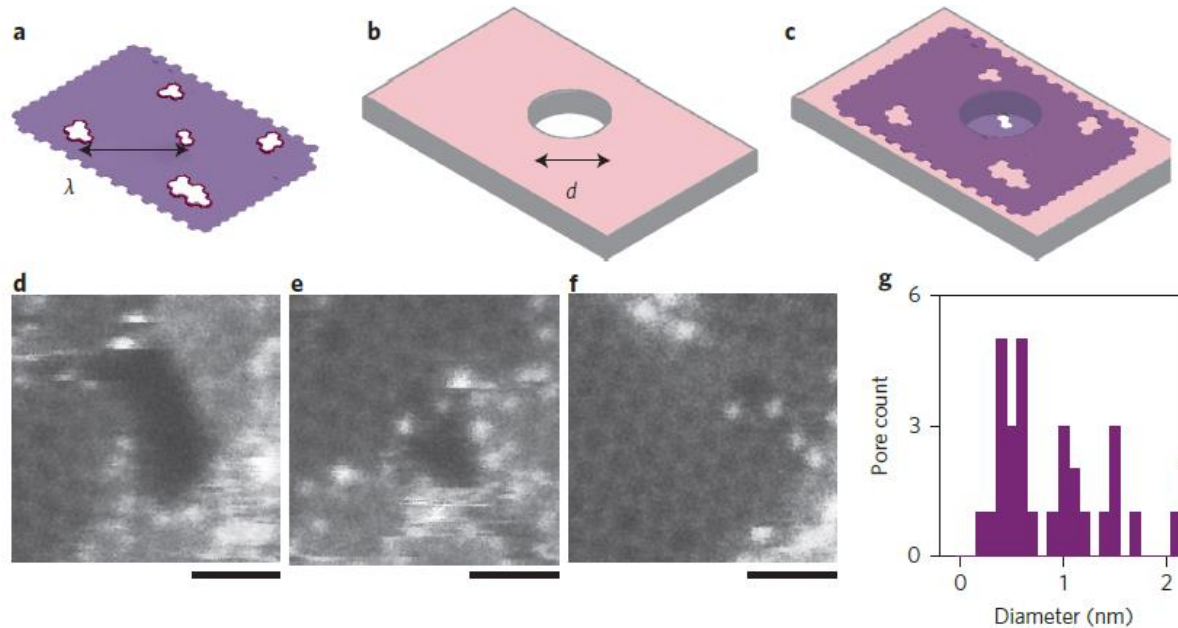
nature
nanotechnology

LETTERS

PUBLISHED ONLINE: 5 OCTOBER 2015 | DOI: 10.1038/NNANO.2015.222

Heterogeneous sub-continuum ionic transport in statistically isolated graphene nanopores

Tarun Jain¹, Benjamin C. Rasera¹, Ricardo Jose S. Guerrero¹, Michael S. H. Boutilier¹, Sean C. O'Hern¹, Juan-Carlos Idrobo² and Rohit Karnik^{1*}



Is it possible to use the experimental techniques used in the presented paper to monitor water movement across graphene hollow nanofibers?



*Do not dwell in the past,
Do not dream of the future,
Concentrate the mind on the present moment.*

- Buddha



Thank
you...